Hindawi Publishing Corporation
Journal of Ceramics
Volume 2013, Article ID 214974, 9 pages
http://dx.doi.org/10.1155/2013/214974

Research Article

Mineral-Oxide-Doped Aluminum Titanate Ceramics with Improved Thermomechanical Properties

R. Papitha,[1] M. Buchi Suresh,[1] Dibakar Das,[2] and Roy Johnson[1]

[1] *Center for Ceramic Processing, International Advanced Research Centre for Powder Metallurgy and New Materials (ARCI), Balapur, Hyderabad 500005, India*
[2] *School of Engineering Sciences and Technology, University of Hyderabad, Hyderabad 500046, India*

Correspondence should be addressed to Roy Johnson; royjohnson@arci.res.in

Received 31 May 2012; Accepted 10 July 2012

Academic Editor: Zhenxing Yue

Investigations were carried out, on the effect of addition of kaolinite ($2Al_2O_3{\cdot}3SiO_2{\cdot}2H_2O$) and talc ($Mg_3Si_4O_{10}(OH)_2$) in terms of bulk density, XRD phases, microstructure, as well as thermal and mechanical properties of the aluminium titanate (AT) ceramics. AT ceramics with additives have shown enhanced sinterability at 1550°C, achieving close to 99% of TD (theoretical density) in comparison to 87% TD, exhibited with pure AT samples sintered at 1600°C, and found to be in agreement with the microstructural observations. XRD phase analysis of samples with maximum densities resulted in pure AT phase with a shift in unit cell parameters suggesting the formation of solid solutions. TG-DSC study indicated a clear shift in AT formation temperature with talc addition. Sintered specimens exhibited significant reduction in linear thermal expansion values by 63% (0.42×10^{-6}/C, (30–1000°C)) with talc addition. Thermal hysteresis of talc-doped AT specimens showed a substantial increase in hysteresis area corresponding to enhanced microcrack densities which in turn was responsible to maintain the low expansion values. Microstructural evaluation revealed a sizable decrease in crack lengths and 200% increase in flexural strength with talc addition. Results are encouraging providing a stable formulation with substantially enhanced thermomechanical properties.

1. Introduction

Aluminum Titanate (Al_2TiO_5, designated as AT) ceramics exhibit excellent thermal properties such as low thermal expansion coefficient in the range of $1.0–1.5 \times 10^{-6}$/C (RT-1000°C) in combination with low thermal conductivity (~1.5 $Wm^{-1}K^{-1}$) and a high melting temperature of 1860°C [1–4]. This makes Al_2TiO_5, a material of choice for many refractory applications. Some of these applications include wall flow filters for diesel particulate emission control, exhaust port liners in automotive engines and thermal shock resistant refractory parts for nonferrous metallurgical industries [5–8]. One of the disadvantages of this ceramic material for practical applications is the low flexural strength due to the extensive microcracks generated whil processing [3, 4, 9]. Crystal structure of aluminum titanate (β-Al_2TiO_5) is pseudo-brookite and is associated with the strong anisotropy in crystallographic axis while heating, which is responsible for microcracking on cooling [9, 10]. The microcracking phenomenon is closely related to the material microstructure. Below a critical grain size, the elastic energy of the system is insufficient for microcrack formation during cooling and thus the mechanical properties are considerably enhanced. Additionally, eutectoid decomposition to its parent oxides such as α-Al_2O_3 and TiO_2 between 750 to 1280°C is also an issue leading to thermal instability of the Al_2TiO_5 phase. This decomposition occurs when the adjacent Al^{3+} (0.54 Å) and Ti^{4+} (0.67 Å) octahedra collapse, because of the lattice site occupied by the Al^{3+} ion is too large. The thermal energy available from this collapse allows Al^{3+} to migrate from its position and causes structural dissolution to rutile (TiO_2) and corundum (α-Al_2O_3) [9–12].

It is also well known that, thermomechanical properties of microcracked ceramics is a function of dopants and many attempts to dope with various oxide compounds (such as MgO, ZrO_2, Fe_2O_3, SiO_2, $ZrSiO_4$) are made so far [13–19]. These oxides are reported to be effective in densification and improving the thermal stability. However, they need

to be doped in high-volume fractions, deteriorating the thermal properties and long-term stability [15]. Doping with spodumene ($LiAlSiO_4$), mullite ($3Al_2O_3{\cdot}2SiO_2$), cordierite ($Mg_2Al_4Si_5O_{18}$), and feldspar have also been attempted, but and no significant enhancement in thermomechanical properties were reported [19–25]. Studies have also attempted to dope with SiO_2 (9 wt%) and co-doping with MgO (10 wt%) and SiO_2 (8 wt%), which have reported significant enhancement in stability and mechanical properties. However, doping with SiO_2 resulted in unreacted residual TiO_2 phase and the formation of additional phases such as $MgAl_2O_4$ and Mg_2SiO_4 with co-doping [17].

In view of the above, the objective of this paper is to elucidate systematically the effect of additives such as kaolinite and talc into Al_2TiO_5 formulation with varying concentrations followed by the evaluation of thermomechanical properties. Accordingly, precursor oxide samples were compacted with and without additives and were subjected to sintering at varying temperatures to achieve close to theoretical density. Sintering behavior of AT was elucidated with dilatometric shrinkage curve and DSC studies. Sintered samples were characterized for their density, phase, microstructure, and CTE measurements. Further, the thermal hysteresis was recorded while heating and cooling using dilatometer. Flexural (3-point bend) strength was also determined and correlated with microcrack densities, observed with fractograph.

2. Experimental Procedure

Basic raw materials such as alumina (Al_2O_3, Baikowski, France) and titania (TiO_2, Qualigens) powders along with the additives kaolinite ($2Al_2O_3{\cdot}3SiO_2{\cdot}2H_2O$) and talc ($Mg_3Si_4O_{10}(OH)_2$) were used for the investigations. XRD phase analysis of the raw materials was carried out by Bruker's D8 advanced system and morphology and particle size analysis by scanning electron microscope (S-4300SE/N, Hitachi, Tokyo, Japan). Physiochemical properties of the raw materials are depicted in Table 1. The concentration of silica (1.5, 3, and 4.5 wt%) in aluminum titanate and sample ID's (C_0, C_1, C_2, C_3, C_4, C_5, and C_6) were depicted in Table 2. The formulations were granulated with 2 wt% of poly vinyl alcohol as a binder and compacted into green compacts of 65 mm × 65 mm × 8 mm using a hydraulic press. The green density of the compacted samples was measured by the dimensional method and was found to be greater than 50% of the theoretical density (estimated by the rule of mixtures). In order to study, the extent of physiochemical changes occurring in green specimens over the processing temperature ranges, the specimens were subjected to the differential scanning calorimetric (DSC) analysis using TG-DSC analyzer (Netzsch, Germany) from room temperature to 1550°C. Basic formulation of Al_2TiO_5 (C_0) has been subjected to dilatometry (Netzsch 402C, Germany) and the shrinkage profile was recorded with respect to the temperature. Three sintering temperatures of 1500°C, 1525°C, and 1550°C were selected for the sintering of all formulations and selection of optimum sintering temperature.

Densities of the samples sintered at different temperatures were evaluated by widely used Archimedes principle (ASTM 792) and phases were analysed by XRD (Bruker's D8 advanced XRD). The polished samples were thermally etched at a temperature, 50°C below the sintering temperature for microstructural observations using a scanning electron microscope (S-4300SE/N, Hitachi, Tokyo, Japan). The specimens were also subjected to dilatometric analysis using a push-rod-type dilatometer (Netzsch 402C, Germany) incorporating the sample holder correction to determine coefficient of linear expansion (CTE). Thermal hysteresis was recorded for the samples of C_0, C_3, and C_5 formulations with additives which have exhibited the highest densities. Sintered samples with the highest densities were also machined to the rectangular specimens of 45 mm × 4 mm × 3 mm for the determination of the flexural strength using 3-point bend test following ASTM C-1161-02C (Instron).

3. Results and Discussion

3.1. Characterisation of Raw Materials. XRD patterns and SEM micrographs of the basic raw materials recorded for Al_2O_3 and TiO_2 used for the present investigations are shown in Figures 1(a), 1(b), 1(c), and 1(d), respectively. XRD pattern of Al_2O_3 indicated the coexistence of α-phase (~85%) as a major phase along with γ-phase (~15%) and TiO_2 powder has shown single anatase phase. SEM micrographs of both the basic powders have shown an irregular morphology with an average particle size of 150 and 300 nm, respectively.

3.2. Characterisation of Sintered Specimens

3.2.1. Densification of Al_2TiO_5 with and without Additives. Variation of bulk densities with sintering temperature for all the compositions is shown in Figures 2(a) and 2(b). It is evident that the bulk density of Al_2TiO_5 formulation without additives has shown only a marginal increase from 84 to 85% of TD with increase of sintering temperature from 1500 to 1550°C. No significant increase in density is observed even at a sintering temperature of 1600°C. Composition, concentration, and sintering temperature are to found have a significant effect on the final density values. Concentrations of both the additives are fixed based on their silica content (Table 1) in such a way that the final formulation corresponds to a silica addition of 1.5, 3, and 4.5% (Table 2). Kaolinite ($2Al_2O_3{\cdot}3SiO_2{\cdot}2H_2O$) addition from 2.9 to 8.8% has resulted in the consistent increase in density from 90% to a maximum density of 99% of TD. Talc ($Mg_3Si_4O_{10}(OH)_2$) addition from 2.5 to 5% increases the density from 92 to 98.63%; however, unlike kaolinite, a higher concentration of talc ($Mg_3Si_4O_{10}(OH)_2$) has not shown any significant increase in density beyond 92%.

Dilatometric curve of Al_2TiO_5 depicted in Figure 3(a) clearly shows an initial shrinkage corresponding to the in-situ reaction sintering of the starting mixture of Al_2O_3 and TiO_2 followed by an expansion regime corresponding to formation of Al_2TiO_5 and is in good agreement with endothermic peak at 1375°C (Figure 3(b)). This expansion regime in

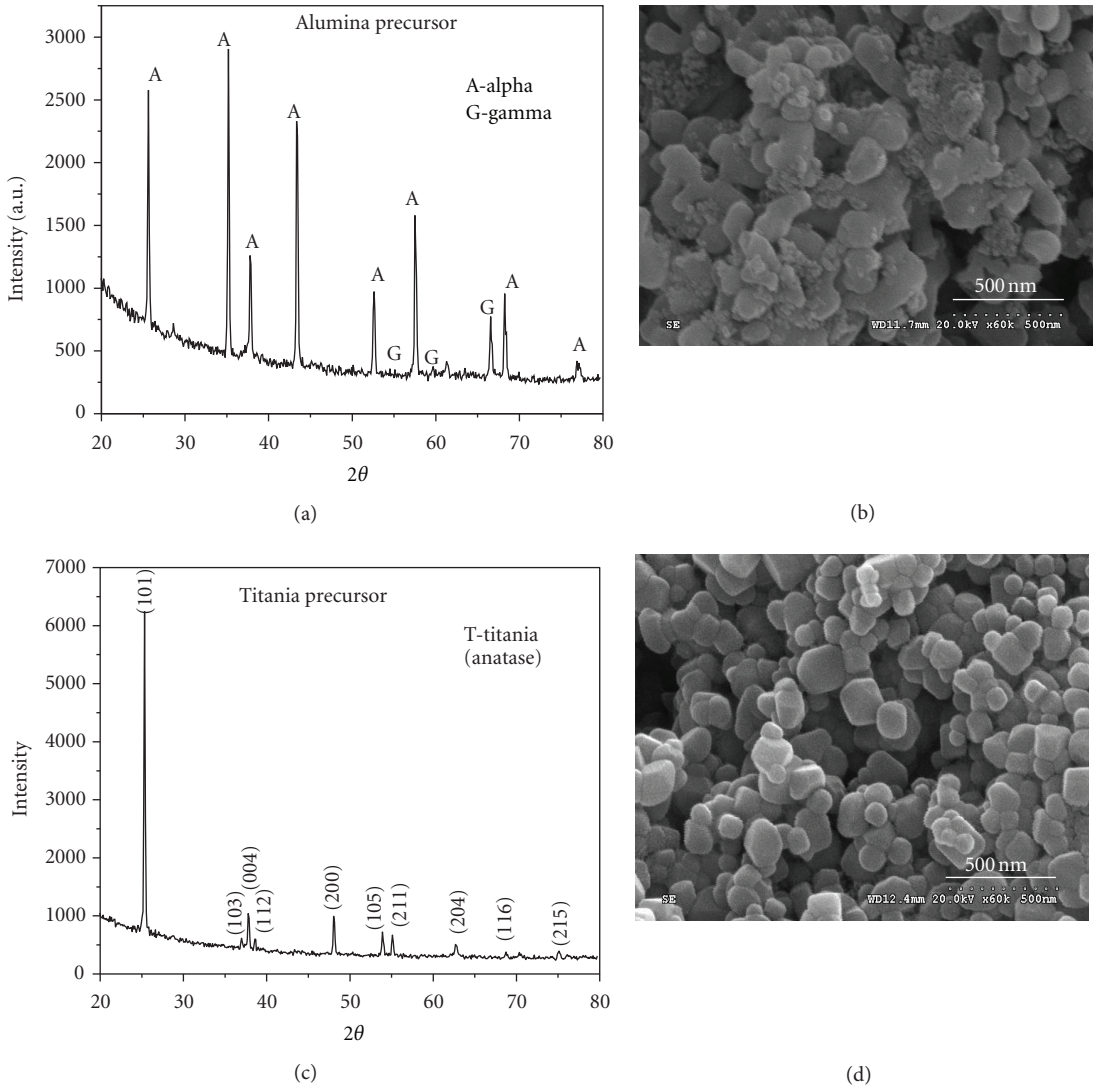

Figure 1: (a) XRD pattern of Al_2O_3 powder, (b) morphology of Al_2O_3 powder, (c) XRD pattern TiO_2 powder, and (d) morphology of TiO_2 powder.

Table 1: Physiochemical properties of raw materials.

Property	Alumina	Titania	Talc	Kaolinite
Chemical composition wt%				
SiO_2			60.0	44.0
Al_2O_3	99.95		2.1	50.2
TiO_2		99.5	0.08	0.4
MgO	0.005		31.1	<0.1
Na_2O			<0.01	0.11
K_2O			<0.01	<0.01
Physical properties				
Average particle size (D_{50})	200 nm	300 nm	21.62 μm	2.86 μm
Crystalline phase	α and γ	Anatase	Talc	Kaolinite

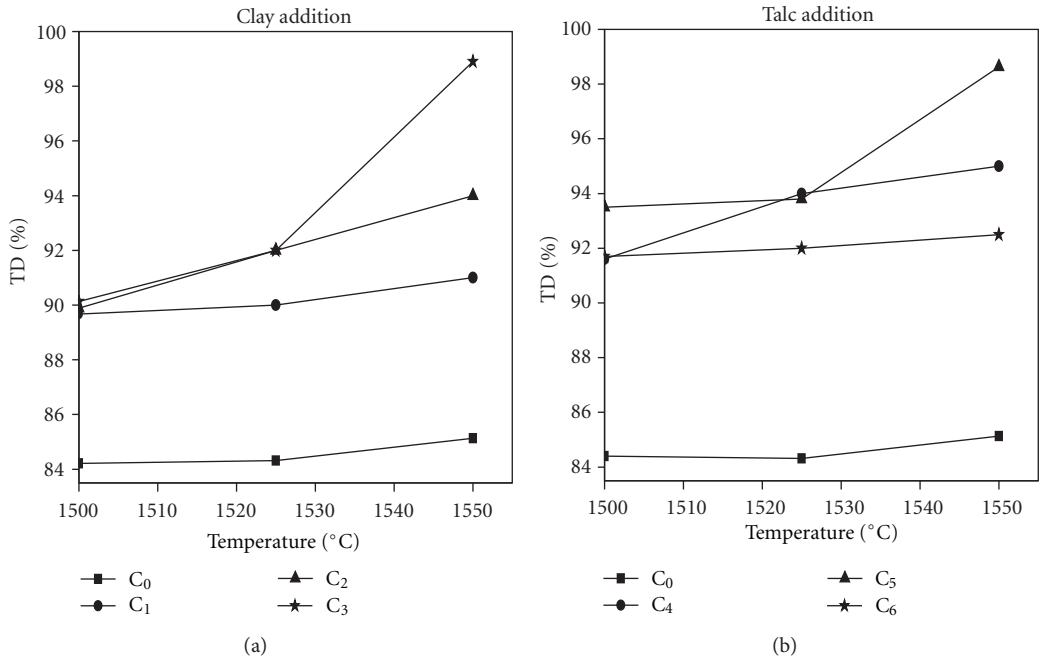

Figure 2: (a) Density variation with temperature of C_0, C_1, C_2, C_3, and (b) Density variation with temperature of C_0, C_4, C_5, and C_6.

Table 2: Formulation investigated (wt%).

Sr. No.	Sample. ID	Al_2O_3	TiO_2	Clay	Talc
1	C_0	56	44	0	0
2	C_1	55.16	43.34	2.94%	0
3	C_2	54.32	42.68	5.88%	0
4	C_3	53.48	42.02	8.82%	0
5	C_4	55.16	43.34	0	2.5%
6	C_5	54.32	42.68	0	5%
7	C_6	53.48	42.02	0	7.5%

fact offsets the densification of AT matrix by around 20%, resulting in poor sintered density of 87% even at a sintering temperature of 1600°C. Endothermic peak at 1386°C for C_3, indicate that there is no significant shift in Al_2TiO_5 phase formation compared to undoped (C_0) formulation (Figure 3(b)). Al_2TiO_5 phase formation temperature is shifted to a lower temperature range of 1274°C for C_5 compared to 1375°C observed with (C_0) un-doped formulation as is evident from the DSC peak (Figure 3(b)).

XRD pattern of the maximum dense sample (C_3) depicted in Figure 4 has not shown any additional peaks and all the peaks could be indexed with standard Al_2TiO_5 phase. However, a shift in unit cell constants is observed in comparison to the pure Al_2TiO_5 samples, especially in the case of "*c*" parameter [10, 17]. The cell parameters and volume of C_0 sample are a = 9.4315 Å, b = 9.6385 Å, c = 3.590 Å, and 326.35 (Å)^3, where as cell parameters and volume of sample C_3 are a = 9.4342 Å, b = 9.6536 Å, c = 3.5940 Å, and 327.32 (Å)^3. The change in unit cell parameter is probably due to silicon (Si^{4+}, ionic radius = 0.41 Å) replacing Al^{3+} in the lattice of Al_2TiO_5 matrix. This may result in the multivalent state for titanium that is, Ti^{3+}/Ti^{4+}, corresponding to a stoichiometry of $((Al^{3+},Ti^{3+})_2(Ti^{4+})_1(O^{2-})_5)$ which in turn enhances the sintering process. A closer look at the micrographs also reveals a change in the porous lamellar type of structure in to relatively dense faceted grains. Further, the microcracks are found visible and crack lengths are reduced to a greater extent in comparison to C_0 with no additives.

XRD pattern of C_5 sample with maximum density depicted in Figure 4 has shown ~96% of Al_2TiO_5 phase with minor quantities of Al_2O_3 after sintering at 1550°C. Further, the TiO_2 peaks are completely absent in the pattern. It is well known that talc ($2MgO{\cdot}2Al_2O_3{\cdot}5SiO_2$) transform to clinoenstatite ($MgSiO_3$) close to 1100°C and at high temperatures, it decomposes to MgO and SiO_2. In the case of C_5 formulation, Mg^{2+} (MgO: 1.5%) and Si^{4+}(SiO_2: 3%)

Table 3: Comparison of CTE values and hysteresis area.

Sample Id	%TD	%AT phase	CTE value (30–1000°C)	Hysteresis area (cm^2)
C_0	85.13	92.04	1.09×10^{-6}/°C	91
C_3	98.9	98	0.94×10^{-6}/°C	68
C_5	98.63	95.5	0.4×10^{-6}/°C	95

Table 4: Comparison of flexural strength and hardness.

Sample	Flexural strength (MPa)	%increase in flexural strength	Hardness (Kg/mm^2)	%increase in hardness
C_0	8.53	—	150	—
C_3	8.61	0.94	180	20%
C_5	25.89	203	200	33.33%

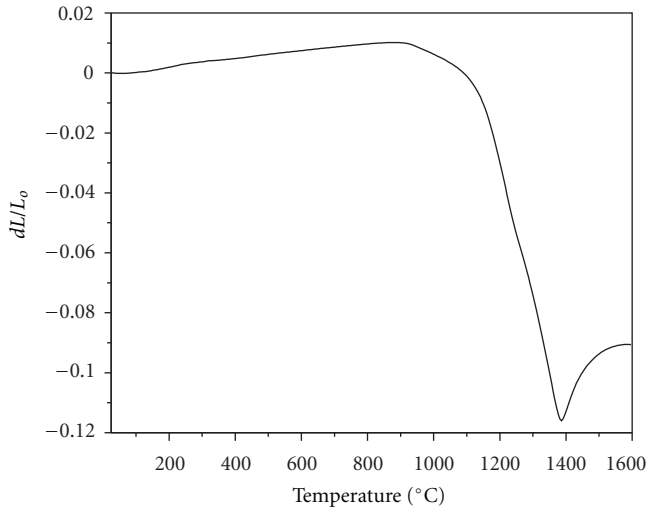

(a)

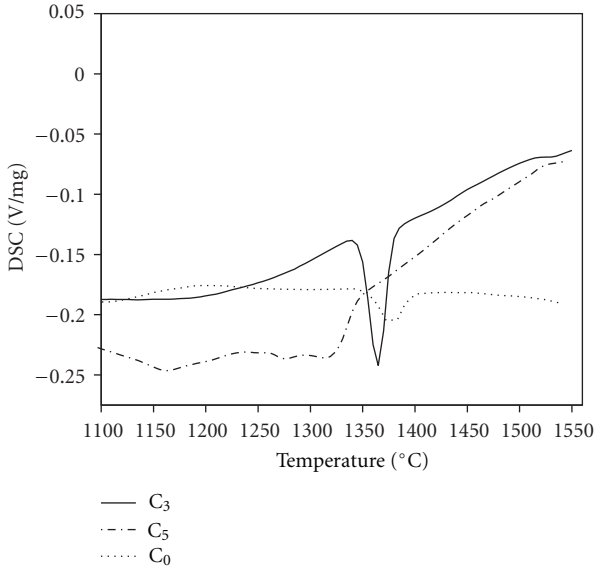

(b)

Figure 3: (a) Shrinkage curve of C_0 and (b) DSC curves C_0, C_3, and C_5.

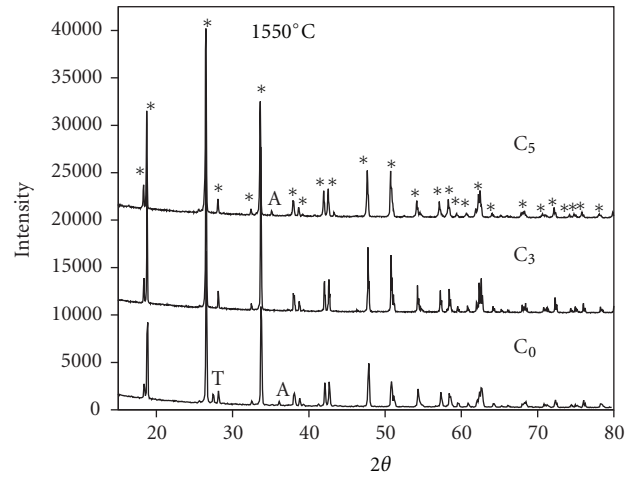

A: Alumina
T: Titania
∗AT: Aluminum titanate

Figure 4: XRD patterns of sintered specimens 1550°C.

ions undergo simultaneous lattice substitutions for Al^{3+} to stabilize Al_2TiO_5 stoichiometry. This leads to change in unit cell parameters due to addition of talc. The unit cell parameters and volume of sample C_0 are $a = 9.4315$ Å, $b = 9.6385$ Å, $c = 3.590$ Å, and 326.35 $(Å)^3$. Whereas in sample C_5 unit cell parameters and volume are $a = 9.4651$ Å, $b = 9.6715$ Å, $c = 3.5981$ Å and 329.37 $(Å)^3$, which displaces the interplanar spaces. The dilation along crystallographic c-axis in talc added samples, further expected to improve phase stability of AT [17]. A larger distortion from the C_0 composition can be attributed to the simultaneous substitution of Si^{4+} (ionic radius = 0.41 Å) and Mg^{2+} (ionic radius = 0.65 Å) replacing Al^{3+} in the lattice of Al_2TiO_5 matrix. Al_2TiO_5 formation process was led by nucleation and growth of grains and finally diffusion of reactant through the matrix and is controlled by the very slow reacting species. In addition to the multivalent state for titanium, that is, Ti^{3+}/Ti^{4+} as a result of Si^{4+} substitution, the presence of Mg^{2+} ions

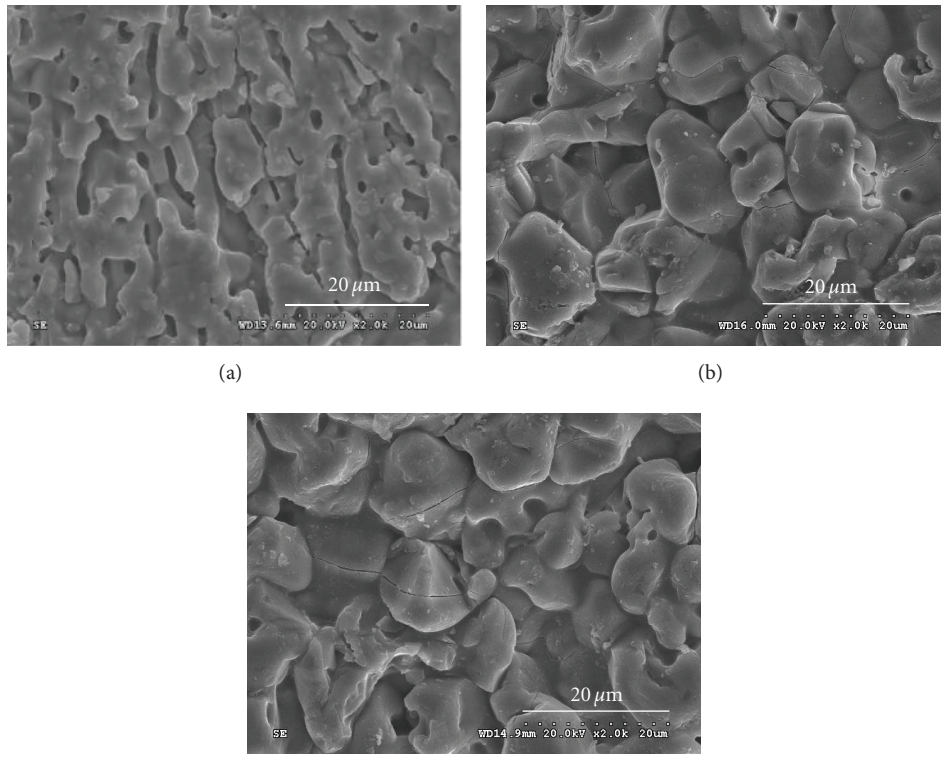

(a) (b)

(c)

Figure 5: (a) SEM microstructure of C_0, (b) SEM microstructure of C_3, and (c) SEM microstructure of C_5.

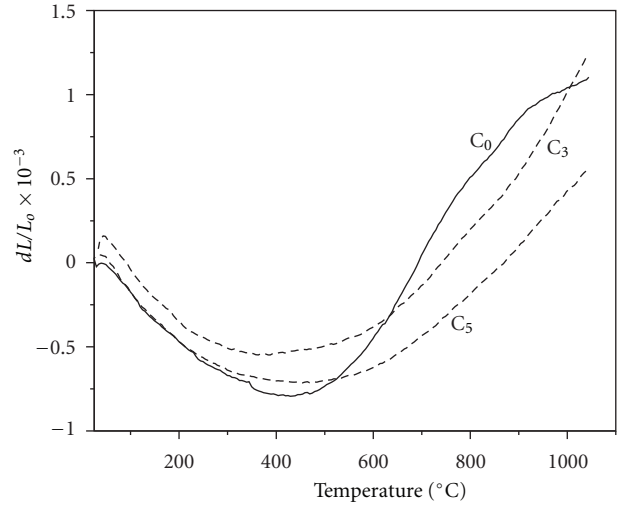

Figure 6: Thermal expansion curves of C_0, C_3, and C_5.

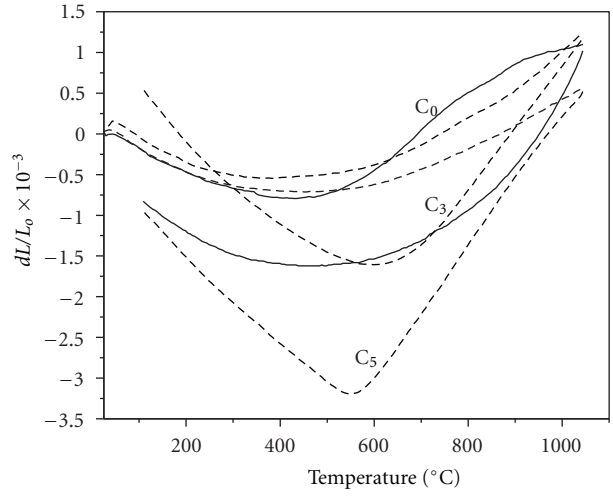

Figure 7: Thermal hysteresis of C_0, C_3, and C_5.

that replaces Al^{3+} may result in oxygen vacancy formation $((Al^{3+},Ti^{3+})_2(Ti^{4+})_1(O^{2-}_{5-\delta})$. These vacancies promote the diffusion in the solid state enhancing densification.

Figures 5(a)–5(c) showed the microstructures of C_0, C_3, and C_5 samples. From the microstructure of C_3 and C_5 samples, it is clear that they possess single AT phase, where as in the case of C_0 some parent residual oxides still exist. Microstructural features do not show any significant variations in the grain size with both the additives (C_3, C_5). However, considerable reduction in intergranular pores is observed with the addition of talc (C_5). The presence of additives enhanced the grain growth in AT ceramics.

3.2.2. Thermal Expansion and Thermal Hysteresis. Dilatometric expansion curve and thermal hysteresis were recorded while heating and cooling of the C_0, C_3, and C_5 samples

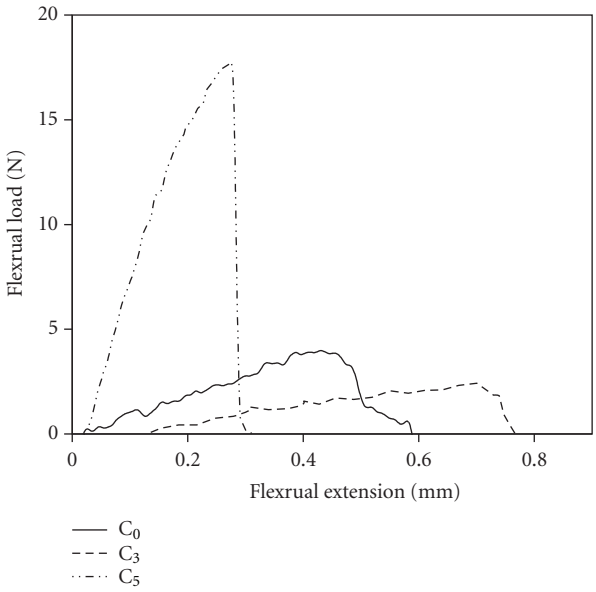

Figure 8: Load-displacement curves of C_0, C_3 and C_5.

were shown in Figures 6 and 7, respectively. Table 3 lists the thermal expansion values of C_0, C_3, and C_5 formulations from 30–1000°C. It is evident that, the formulation C_0 has a CTE value of 1.09×10^{-6}/°C followed by $C_3$with a marginally lower CTE value of 0.94×10^{-6}/°C(13% less than C_0) and the lowest value of 0.42×10^{-6}/°C (63% less than C_0) for C_5 formulation. Thermal expansion curves of the entire samples initially contract till 450°C. Thermal expansion curves of C_0 exhibit a dissimilar behavior in comparison with C_3 and C_5 formulation. C_0 sample exhibited a low expansion of -1.97×10^{-6}/°C in comparison to C_3 and C_5 for which CTE values are -1.71×10^{-6}/°C and -1.74×10^{-6}/°C, respectively. All samples have shown an expansion behavior beyond 450°C and C_0 exhibited a significant slope change leading to the maximum expansion value. The temperature, beyond which the expansion becomes prominent, was regarded as the temperature at which healing of microcracks occurs that compensates the expansion effectively. Further, the curves corresponding to C_0 are tapered into a plateau beyond 900°C unlike other samples with a positive slope.

Cooling curves also behaved differently with all the three samples. C_0 formulation has shown a negative slope tapering into a plateau followed by the expansion. Initial contraction had α values of 6.08, 7.75, and 3.04×10^{-6}/°C (temperature regime, 1000–450°C) and final expansion region had α values of -4.37, -7.75, and -2.3×10^{-6}/°C (temperature regime, 450–100°C) for C_5, C_3, and C_0 respectively. Expansion below 450°C can be attributed to the reintroduction of micro-cracks healed while heating.

It is obvious that thermal properties of doped and undoped Al_2TiO_5 ceramics are mainly governed by the presence of microcracks and are affected by the crack closure or healing. Areas of the thermal hysteresis were recorded during heating up to 1000°C and cooling up to 100°C for formulations of C_5, C_3, and C_0 were 95, 68 and 91 cm^2, respectively. Unlike other samples, C_3 showed two closed loops where first loop is in the temperature regime of 1000 to 300°C, which had dL/L_0 value less than dL/L_0 value of sample while heating, as expected. However, the second loop formed at 300°C, exhibited a higher dL/L_0 value which is unusual. Probably this may be due to the transformation of microcracks into macro cracks due to high silica content (4.5%) leading to a relatively low hysteresis area of 68 cm^2 observed with C_3 sample in comparison to 91 cm^2observed with C_0 sample having close CTE values [17]. C_5 sample exhibited hysteresis area of 95 cm^2, which correlates well with the low CTE value (0.42×10^{-6}/°C) as a result of compensation of expansion values. Microcrack density (number of microcracks/unit area estimated using several SEM images) of C_5 sample was almost 3 times of that of the C_0 sample confirming the above observations.

3.2.3. Flexural Strength and Hardness Measurements. Typical load-displacement curves obtained from the specimens C_0, C_3 and C_5 which were subjected to 3-point bend loading and is shown in Figure 8. Though a minimum of 4-5 specimens were tested in each case, for the sake of clarity, only one load-displacement curve for each condition are shown. Flexural strength (σ_f) is calculated from the load displacement data as $\sigma_f = 3/2PL/bd^2$, where P_{max} is the maximum load, L the span length, b the width, and d the thickness of the specimens. The flexural strength values are given in Table 4. C_5 with talc doping exhibited the peak flexural strength before fracture (average, 28 ± 3 MPa) which is ~200% higher than the corresponding flexural strength values (average 8 ± 4 MPa) of the C_3 and C_0 samples. It is evident from the data in Figure 8 that C_0 and C_3 materials show a similar unstable crack extension with load drop after attaining peak flexural stress. A close look at the load-displacement curves obtained from the flexural loading of the C_3 and C_0 samples (shown in Figure 8) has shown several load excursions while on attaining peak load depicting fracture over a wide range of strain followed by a gradual load drop. Poor strength in fracture behavior even with a high density (99% of TD) can be attributed to increase in crack length and more number of macrocracks (crack length up to 30 μm, Figure 5(b)). It is obvious that poor density (85%) and the high porosity are the factors that contribute in addition to the microcracks to the identical fracture behavior observed with C_0 compositions.

Unlike the other samples, C_5 composition exhibited initial rapid increase in the stress, reaching a peak value followed by the fracture. It is clear that, prior to the attainment of the peak flexural stresses, the material showed almost a linear increase in flexural stress with strain, indicating elastic deformation, before final failure. This can be attributed to the association of the existing large number of micro cracks (Figure 5(c), microcracks are restricted within the grain with maximum crack length <10 μm) leading to the stable crack extension. Finally, the material fails with sudden load drop, which is an indication of rapid propagation of the macrocracks that resulted from coalescence of large number

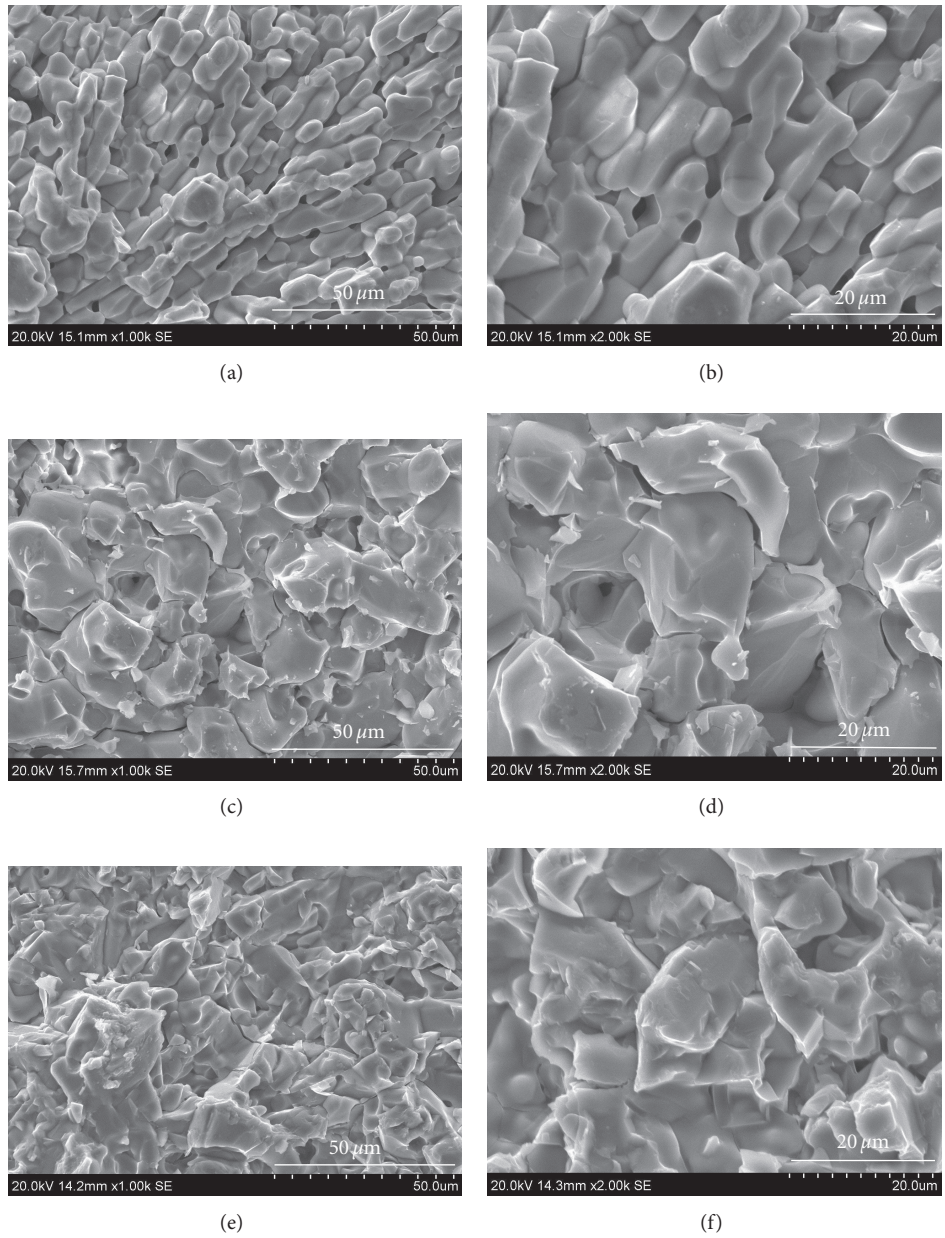

FIGURE 9: (a)-(b) Fractography microstructure of C_0 at different magnifications, (c)-(d) fractography microstructure of C_3 at different magnifications, and (e)-(f) fractography microstructure of C_5 at different magnifications.

of micro cracks under local tensile loading. Hardness of the specimens C_3 and C_5 has shown an enhancement 20% and 33.3% with respect to C_0. A relatively high hardness under identical densities could attribute to the marginal decrease in grain size observed with C_5 samples.

SEM fractographs obtained from the specimens C_0, C_3, and C_5 tested till the failure under flexural (3-point bend loading) testing are shown in Figures 9(a)–9(f). Though large number of fractographs at different magnifications is obtained in each of the specimen, for the sake of clarity, only one representative fractograph is depicted. These fractographs show an identical transgranular fracture. As discussed above, C_5 composition is associated with more microcracks and the crack path while propagation needs to relocate for further crack extension as it encounters more and more microcracks. Such process needs higher fracture energy as compared to the C_0 and C_3 where microcrack densities were low.

4. Conclusions

Addition of kaolinite ($2Al_2O_3.3SiO_2.2H_2O$) and talc ($Mg_3Si_4O_{10}(OH)_2$) in relatively low concentration of 8.8 wt% and 5 wt%, respectively, resulted in enhanced densification leading to a substantial increase in percentage theoretical density to 99% in comparison with pure Al_2TiO_5 with 87%

processed under identical conditions. Kaolinite and/or talc substitution results in multivalent titanium (Ti^{3+}/Ti^{4+}) and oxygen vacancies in Al_2TiO_5 formulations promoting the enhanced diffusion and densification. Microstructural evaluations revealed transformation of porous lamellar type of structure of pure Al_2TiO_5 into relatively dense faceted grains with kaolinite and talc confirming higher density values. XRD studies have shown an improvement in Al_2TiO_5 phase content from 92% to a maximum of 98% with the addition of kaolinite. The enhancement in phase content was moderate in case of talc with a maximum of 95.5%; however, DSC studies indicated a drop of ~85°C in phase formation temperature. Substantial improvement in thermomechanical properties was observed with talc addition in comparison to kaolinite. A decrease in thermal expansion value of Talc-doped AT by 63% and an enhancement of flexural strength value by 200% is demonstrated in the present study. These properties found to have a good correlation with the presence and the mode of microcracks as revealed by microstructure and thermal hysteresis. Talc-doped Al_2TiO_5 formulation presently developed with superior thermomechanical properties can be explored for various potential applications.

References

[1] M. Nagano, S. Nagashima, H. Maeda, and A. Kato, "Sintering behavior of Al_2TiO_5 base ceramics and their thermal properties," *Ceramics International*, vol. 25, no. 8, pp. 681–687, 1999.

[2] G. Bruno, A. M. Efremov, B. R. Wheaton, and J. E. Webb, "Microcrack orientation in porous aluminum titanate," *Acta Materialia*, vol. 58, no. 20, pp. 6649–6655, 2010.

[3] R. Naghizadeh, H. R. Rezaie, and F. Golestani-fard, "The influence of composition, cooling rate and atmosphere on the synthesis and thermal stability of aluminum titanate," *Materials Science and Engineering B*, vol. 157, no. 1–3, pp. 20–25, 2009.

[4] K. Hamano, Y. Ohya, and Z. E. Nakagawa, "Crack propagation resistance of aluminium titanate ceramics," *International Journal of High Technology Ceramics*, vol. 1, no. 2, pp. 129–137, 1985.

[5] H. C. Kim, K. S. Lee, O. S. Kweon, C. G. Aneziris, and I. J. Kim, "Crack healing, reopening and thermal expansion behavior of Al_2TiO_5 ceramics at high temperature," *Journal of the European Ceramic Society*, vol. 27, no. 2-3, pp. 1431–1434, 2007.

[6] Y. X. Huang and A. M. R. Senos, "Effect of the powder precursor characteristics in the reaction sintering of aluminum titanate," *Materials Research Bulletin*, vol. 37, no. 1, pp. 99–111, 2002.

[7] G. Bruno, A. Efremov, B. Wheaton, I. Bobrikov, V. G. Simkin, and S. Misture, "Micro- and macroscopic thermal expansion of stabilized aluminum titanate," *Journal of the European Ceramic Society*, vol. 30, no. 12, pp. 2555–2562, 2010.

[8] C. H. Chen and H. Awaji, "Temperature dependence of mechanical properties of aluminum titanate ceramics," *Journal of the European Ceramic Society*, vol. 27, no. 1, pp. 13–18, 2007.

[9] B. Morosin and R. W. Lynch, "Structure studies on Al_2TiO_5 at room temperature and at 600°C," *Acta Crystallographica B*, vol. 28, pp. 1040–1046, 1972.

[10] R. D. Skala, D. Li, and I. M. Low, "Diffraction, structure and phase stability studies on aluminium titanate," *Journal of the European Ceramic Society*, vol. 29, no. 1, pp. 67–75, 2009.

[11] A. Durán, H. Wohlfromm, and P. Pena, "Study of the behaviour of Al_2TiO_5 materials in reducing atmosphere by spectroscopic techniques," *Journal of the European Ceramic Society*, vol. 13, no. 1, pp. 73–80, 1994.

[12] I. M. Low, Z. Oo, and B. H. O'Connor, "Effect of atmospheres on the thermal stability of aluminium titanate," *Physica B*, vol. 385-386, pp. 502–504, 2006.

[13] V. Buscaglia, P. Nanni, G. Battilana, G. Aliprandi, and C. Carry, "Reaction sintering of aluminium titanate: i-effect of MgO addition," *Journal of the European Ceramic Society*, vol. 13, no. 5, pp. 411–417, 1994.

[14] A. Yoleva, S. Djambazo, D. Arseno, and V. Hristo, "Effect of SiO_2 addition on thermal hysteresis of aluminum titanate," *Journal of University of Chemical Technology and Metallurgy*, vol. 45, no. 3, pp. 269–274, 2010.

[15] H. A. J. Thomas, R. Stevens, and E. Gilbart, "Effect of zirconia additions on the reaction sintering of aluminium titanate," *Journal of Materials Science*, vol. 26, no. 13, pp. 3613–3616, 1991.

[16] T. Korim, "Effect of Mg^{2+}- and Fe^{3+}-ions on formation mechanism of aluminium titanate," *Ceramics International*, vol. 35, no. 4, pp. 1671–1675, 2009.

[17] J. Lan, C. Xiao-Yan, H. Guo-Ming, and M. Yu, "Effect of additives on properties of aluminium titanate ceramics," *Transactions of Nonferrous Metals Society of China*, vol. 21, no. 7, pp. 1574–1579, 2011.

[18] I. J. Kim, K. S. Lee, and G. Cao, "Low thermal expansion behavior of $ZrTiO_4$-Al_2TiO_5 ceramics having high thermal durability between 750 and 1400°c," *Key Engineering Materials*, vol. 22, pp. 2627–2632, 2002.

[19] L. Giordano, M. Viviani, C. Bottino, M. T. Buscaglia, V. Buscaglia, and P. Nanni, "Microstructure and thermal expansion of Al_2TiO_5-$MgTi_2O_5$ solid solutions obtained by reaction sintering," *Journal of the European Ceramic Society*, vol. 22, no. 11, pp. 1811–1822, 2002.

[20] T. Shimada, M. Mizuno, K. Katou et al., "Aluminum titanate-tetragonal zirconia composite with low thermal expansion and high strength simultaneously," *Solid State Ionics*, vol. 101–103, no. 1, pp. 1127–1133, 1997.

[21] P. Oikonomou, C. Dedeloudis, C. J. Stournaras, and C. Ftikos, "Stabilized tialite-mullite composites with low thermal expansion and high strength for catalytic converters," *Journal of the European Ceramic Society*, vol. 27, no. 12, pp. 3475–3482, 2007.

[22] A. Tsetsekou, "A comparison study of tialite ceramics doped with various materials and tialite-mullite composites: microstructural, thermal and mechanical properties," *Journal of the European Ceramic Society*, vol. 25, no. 4, pp. 335–348, 2005.

[23] F. H. Perera, A. Pajares, and J. J. Meléndez, "Strength of aluminium titanate/mullite composites containing thermal stabilizers," *Journal of the European Ceramic Society*, vol. 31, no. 9, pp. 1695–1701, 2011.

[24] C. G. Shi and I. M. Low, "Use of spodumene for liquid-phase-sintering of aluminium titanate," *Materials Letters*, vol. 36, no. 1–4, pp. 118–122, 1998.

[25] C. G. Shi and I. M. Low, "Effect of spodumene additions on the sintering and densification of aluminum titanate," *Materials Research Bulletin*, vol. 33, no. 6, pp. 817–824, 1998.